SCIENTIFIC REPORTS

OPEN

Thermal carbonization in nanoscale reactors: controlled formation of carbon nanodots inside porous $CaCO_3$ microparticles

Received: 14 November 2017
Accepted: 14 May 2018
Published online: 20 June 2018

Anna V. Vostrikova[1], Ekaterina S. Prikhozhdenko[1], Oksana A. Mayorova[1], Irina Yu. Goryacheva[1], Nadezda V. Tarakina[2], Gleb B. Sukhorukov[1,2] & Andrei V. Sapelkin[1,3]

Synthesis of carbon nanodots (CNDs) in confined geometry via incorporation of dextran sulphate into pores of $CaCO_3$ microparticles is demonstrated. The preparation process included three steps: co-precipitation of solutions of inorganic salts and carbon source, thermal treatment and $CaCO_3$ matrix removal. We show that geometric constraints can be used to precisely control the amount of source material and to avoid formation of large carbon particles. Analysis of TEM data shows particle size of ~3.7 nm with narrow size distribution. Furthermore, we found that variation in pore morphology has a clear effect on CNDs structure and optical properties. CNDs with graphene oxide like structure were obtained in the nanoporous outer shell layer of $CaCO_3$ microparticles, while less ordered CNDs with the evidence of complex disordered carbons were extracted from the inner microcavity. These results suggest that confined volume synthesis route in CaCO3 nanopores can be used to precisely control the structure and optical properties of CNDs.

Light emitting carbon nanodots (CNDs) have recently emerged as a new family of low dimensional nanocarbon materials. Compared to the more conventional light emitting quantum dots (e.g. CdSe, CdS, Si and Ge etc.), CNDs have clear advantages[1–4] such as low environmental impact, low cytotoxicity, excitation-dependent emission wavelength, excellent biocompatibility, tunable surface functionalities, stability under ambient conditions. These appealing properties of CNDs suggest great opportunities for applications ranging from consumer electronics[5], to light harvesting[6–8] and biological cell imaging[7]. As a consequence, the field has been growing rapidly with thousands of articles published over the last few years. One of the major approaches to synthesis of CNDs is "bottom-up" preparation of structured materials via controlled assembly of atoms and molecules. This approach allows the synthesis of CNDs from a wide variety of molecular precursors - mainly carbon sources with diverse properties and composition. Vast majority of the synthesis routes involve high-temperature treatment options: pyrolysis[9], ultrasonic[4,10–12] or microwave radiation[13–18], solvotermal[19,20] and hydrothermal carbonization methods[21–24]. The latter route being particularly wide-spread due to its relative simplicity. The main problems arising in the synthesis of CNDs are non-uniformity in morphology and size distribution, formation of by-products, in particular, large carbon particles[8,25–29]. The heterogeneous nature of the reaction products is a consequence of relatively poor control over the synthesis environment since the molecular diffusion, temperature fluctuations and particle growth conditions cannot be effectively controlled on the nanoscale level in large volume reactors.

Micro- and nano-porous structures are a promising type of synthesis environment because of a possibility to perform reaction in a restricted volume with precisely controlled amount of reagents. There are a number of advantages in using porous structures as reaction volumes such as varying the size and morphology of the pores and access to a variety of matrixes (including metals, silica, inorganic and organic particles[30–32] and polymers[33,34]). Furthermore, pore geometry may have a significant effect on carbon-based systems in particular by influencing preference for configurations with sp, sp^2 and sp^3 hybridizations (bonding) and hence can be used to control the atomic structure and functionality of the final product.

[1]Saratov State University, 83 Astrakhanskaya Street, Saratov, 410012, Russia. [2]School of Engineering and Materials Science, Queen Mary University of London, Mile End Road, London, E1 4NS, UK. [3]School of Physics and Astronomy, Queen Mary University of London, Mile End Road, London, E1 4NS, UK. Correspondence and requests for materials should be addressed to A.V.S. (email: a.sapelkin@qmul.ac.uk)

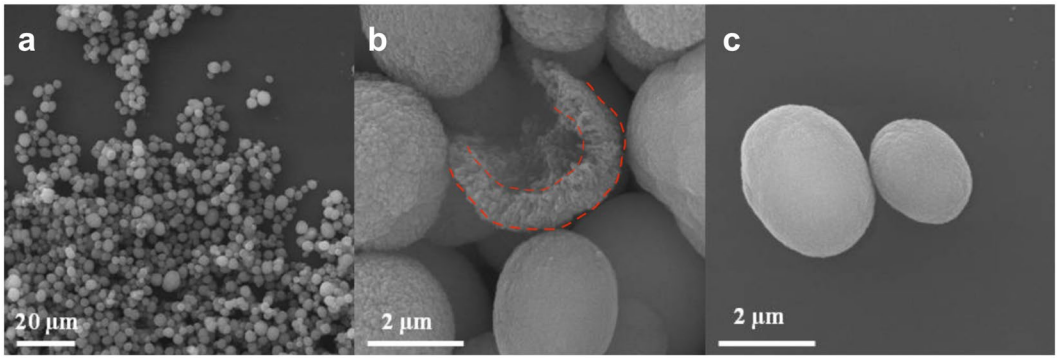

Figure 1. SEM images of $CaCO_3$ microparticles (**a**), and of a broken particle (**b**) (with the shell structure outlined by the dashed red lines); the size and the surface morphology of DS-loaded $CaCO_3$ microparticles is also shown (**c**).

Porous structures have already been used for preparation of CNDs utilizing, for example, impregnation of mesoporous silica[35]. However, there are a number of significant disadvantages using mesoporous silica as a reaction volume which may restrict their commercial potential: the complexity of sample preparation within the mesoporous silica, complexity of removing the host material (etching with concentrated HF[36] or NaOH[37]), and the undefined yield of the reaction product because of distribution of carbon source between pores and bulk solution. The impregnation is also associated with large losses of carbon material when only an impregnating solution inside the pores takes part in CNDs formation[36].

At the same time, polymeric systems[38] have already been used as a synthesis template while $CaCO_3$ microparticles currently attract a lot of attention due to their ability to encapsulate various substances, controlled permeability, high surface-to-volume ratio and sufficient thermal stability. In this context, polycrystalline vaterite particles have a convenient spherical shape, developed surface and high porosity. The diameter of $CaCO_3$ particles is typically from 1 to 6 µm[39], the pore size is in the range of 20–70 nm and they are extensively used in engineering and bioengineering, chemical technology and are already compatible with the commercial manufacturing processes[40–43]. Besides, they are non-toxic and suitable for drug delivery systems development[44]. A significant advantage of these microreactors is the possibility of their removal under relatively mild conditions, using a solution of ethylenediaminetetraacetic acid[45] or hydrochloric acid[46].

In this work, we report a controlled formation of hydrophilic CNDs in pores of $CaCO_3$ microparticles as a result of co-precipitation of inorganic salts ($CaCl_2$ and Na_2CO_3) and sodium dextran sulfate (DS) as a carbon source, followed by thermal treatment. DS was chosen as carbon source because it is a non-toxic natural polymer, based on anhydroglucose and is routinely used for the selective precipitation of lipoproteins. We show that synthesis in a restricted volume has a clear effect on the structure and light emission in CNDs.

Results and Discussion

$CaCO_3$ microparticles with a spherical shape, porous structure and narrow size distribution (3–4 µm, Fig. 1a) were manufactured and used as the templates for CNDs synthesis. The cross-section image (Fig. 1b) further confirms the porous structure of the microparticles. One can also clearly see frequently observed[47] shell-like structure (see broken red lines in Fig. 1b) of the $CaCO_3$ microparticles which makes it possible to vary controllably synthesis conditions (i.e. degree of confinement of the ingredients) across the volume. The lower surface roughness of DS-loaded $CaCO_3$ microparticles ($CaCO_3$–DS, Fig. 1c) reflects presence of DS in $CaCO_3$ microparticles and indirectly corroborates DS co-precipitation within $CaCO_3$. This is further confirmed by confocal fluorescence imaging that shows presence of the light emitting material throughout the volume and the surface of $CaCO_3$ microparticles (Fig. S1).

After thermal treatment $CaCO_3$–DS microparticles colour has changed from white to brown while no soot was formed (Fig. S2). We examined photoluminescence (PL) from CNDs obtained in $CaCO_3$ at various DS concentrations (2, 5 and 10 mg/ml) and did not observe significant differences between the spectra for the corresponding fractions at a given excitation wavelength (Fig. S3). Consequently, we only carried out further detailed analysis of the samples with initial DS concentration of 2 mg/ml. We also performed hydrothermal treatment of DS solutions (under identical temperature conditions) for reference where outcomes were clearly different: colour has changed to the dark-brown, soot was formed, while amount of soot (Fig. S4) and light emission (Fig. S5) were dependent on DS concentration.

Following the synthesis, CNDs were extracted from the $CaCO_3$ surface layer (fraction 1), intermediate layer (fraction 2) and the core region (fraction 3) of microparticles (Fig. 2a) and examined using TEM. We found that average particle sizes are similar (~3.7 nm) for all fractions (Figs 2c–e and S6). The sample obtained in a homogeneous solution of DS in water does not show the formation of particles (Fig. 2f) and is clearly different from those samples that have been extracted from $CaCO_3$–DS microparticles.

Selected area electron diffraction (SAED) data (Figs 2b and S7) for all fractions show a number peaks that can be attributed to small crystallites of $Ca(OH)_2$, possibly formed on a TEM grid while drying. All fractions show peaks corresponding to 2.1 Å (0.48 $Å^{-1}$, close to the graphene sheet 100 reflection value 2.1 Å), while fraction 1 has a broad peak (marked with an star) at 2.40 Å (0.42 $Å^{-1}$, close to 1120 reflection in graphite and graphene oxide

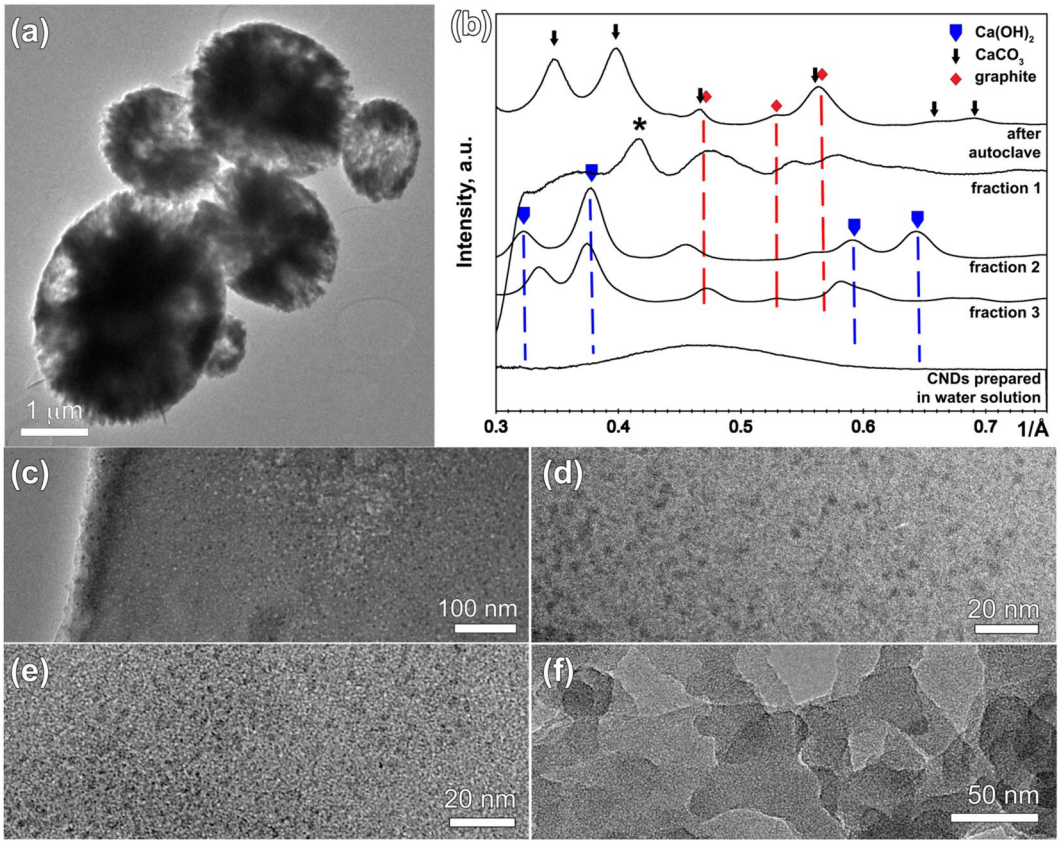

Figure 2. TEM images of (**a**) CaCO3-DS microcapsules (DS initial concentration 2 mg/ml); (**b**) azimuthal average profiles of SAED patterns collected from microcapsules; TEM images obtained from (**c**) fraction 1, (**d**) fraction 2, (**e**) fraction 3 and (**f**) from samples synthesized in water solution.

at 2.46 Å) corresponding to the lattice planes observed in graphene and graphene oxide quantum dots[48]. Only fraction 3, obtained from the core of the $CaCO_3$ particles, has the reflection that corresponds to the interlayer spacing in graphite (3.46 Å, 0.28 $Å^{-1}$, 002 reflection, Fig. S8). One can also see that there is a much closer similarity between SAED patterns of fractions 2 and 3 than between them and fraction 1. CNDs prepared in water solution show amorphous-like diffraction pattern with no clear reflections. To aid further understanding of the atomic structure of samples we performed Raman measurements.

In carbon systems Raman data can provide valuable information on the level of structural ordering owning to resonant excitations of π states. Raman can also be used to trace the variation from single layer, to graphite-like, through to nanocrystalline graphite and amorphous carbons and thus to evaluate the relative fractions of sp^2 and sp^3 bonded structures[49–53]. We found that Raman spectra for the three selected fractions are distinctively different (Fig. 3a). Samples extracted from the shell clearly show D band around 1350 cm^{-1} (K-point phonons of A_{1g} symmetry, defect band) and G band around 1580–1600 cm^{-1} (zone center phonons of E_{2g} symmetry). The G-band involves the in-plane bond-stretching motion of pairs of sp^2-bonded C atoms and does not require the presence of six-fold rings. At the same time, the D band is a breathing mode that is forbidden in perfect graphite structures and only becomes active in the presence of disorder (including surface contribution in the case of small particles). Its intensity is proportional to the number of six-fold aromatic rings (for which the defect band is active), while broadening of D band reflects disorder in such clusters. Raman spectrum of fraction 1 demonstrates clearly distinguishable and relatively narrow D and G bands which are similar to the Raman signal observed in graphene oxide[53,54]. The broadening of D-band and gradual reduction in the relative intensity (i.e. I_D/I_G ratio) of the D and G bands in the spectra of fractions 2 and 3 corresponds to increasing bond-angle disorder and reduction in the number of six-fold rings in the structure of these fractions[50]. We detected two types of spectra (designated as fraction 2a and 2b in Fig. 3a) for the fraction 2 with the spectral features showing gradual broadening of D and G bands and reduction in the relative intensity of the D band. This is the result of probing a larger sample volume compared to the TEM measurements and suggests that fraction 2 may be structurally intermediate between fractions 1 and 3. The gradual broadening of the G band is the consequence of growing disorder of sp^2-bonded sites, while drop in G band intensity indicates reduction of relative proportion of sp^2-bonded sites[50] (i.e. increase in sp^3-bonding character). Thus, although fractions 2 and 3 do also exhibit two major peaks associated with D and G bands (1354 cm^{-1} and 1590 cm^{-1}), they are clearly more complex systems with broader peaks, while also showing additional features at around 1200 cm^{-1} and 1450 cm^{-1} (marked with arrows). The shoulder at around 1200 cm^{-1} is frequently observed in nanodiamonds[54,55], but features in this range can also be associated[56] with C-C stretching modes in hydrocarbon chains. The feature observed at around 1450 cm^{-1} can be assigned to CH_2

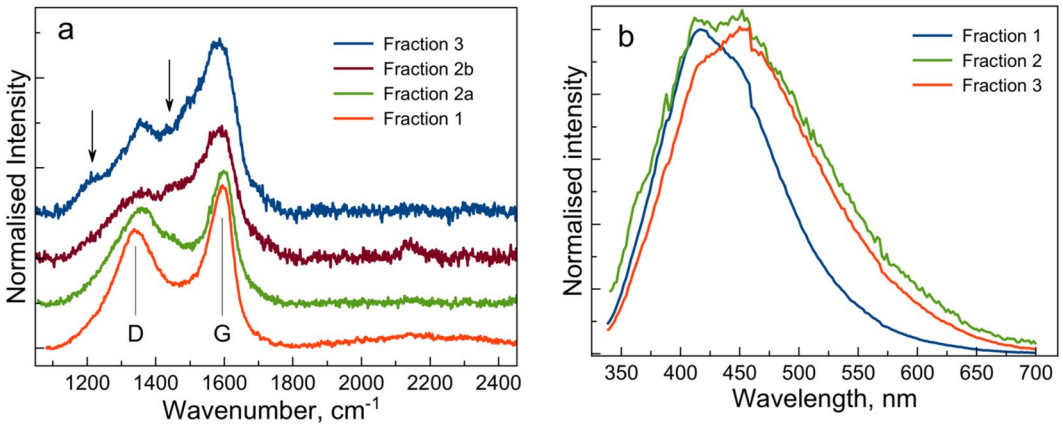

Figure 3. (**a**) Raman data for fractions 1, 2 and 3. Two different spectra (designated Fraction 2a and Fraction 2b) were observed for the fraction 2. Features at around 1200 cm^{-1} and 1450 cm^{-1} are marked with arrows. (**b**) Normalized PL data for all three fractions are also shown (exc. 320 nm).

scissoring mode[57]. Thus, we find that the Raman data are consistent with the SAED results showing more complex spectra for fractions 2 and 3 and hence a clear influence of the reaction volume configuration on CNDs' structure. Furthermore, features of both fraction 1 and fraction 3 can be found in the fraction 2 (Fig. 3a).

This trend in variation of physical properties of CNDs across $CaCO_3$ microparticles volume is also observed in PL spectra recorded for all three fractions (Fig. 3b). One can see a clear shift of the PL peak maximum for fractions 1 to 3, while fraction 2 contains both peaks. Interestingly, in our measurements this trend is observed for the PL data recorded in colloidal water suspension of CNDs where PL has been found to be governed by the surface states rather than by the carbon core[38]. This suggests variations in the surface structure across fractions, which is consistent with the Raman and SAED data.

Thus, experimental data clearly show a systematic variation of structure and light emission in CNDs prepared inside nanopores of $CaCO_3$ microparticle with samples extracted from well-defined porous layers. Furthermore, we show that thus prepared CNDs are structurally different from those synthesized in DS solution in water where amorphous-like structure is observed. We believe that similarity of the Raman and TEM data for the obtained structures with those reported for CNDs prepared by hydrothermal synthesis route[23] may suggest a similar formation mechanism: DS dehydration, followed by polymerization and finally formation of CNDs in $CaCO_3$ pores that act as nanoscale reaction volumes. However, synthesis within the confined volume of nanoscale pores in $CaCO_3$ microparticles allows to control precisely the amount of precursors and shows a clear effect on particle size and size distribution (see Fig. S6).

Conclusions

In conclusion, we demonstrated a relatively simple method of synthesis of hydrophilic CNDs in pores of $CaCO_3$ microparticles using DS as a carbon source. The results clearly show that light emission does not depend on initial concentration of DS in the 2–10 mg/ml range, while the restriction of the reaction volume can be used to influence CNDs structure and light emission and to avoid formation of large microparticles. TEM, SAED, Raman and PL data all point to the influence of pore morphology on the structural properties and light emission in CNDs. CNDs with graphene oxide like structure were obtained in the nanoporous outer shell layer of $CaCO_3$ microparticles, while less ordered CNDs with the evidence of complex disordered carbons were extracted from the inner microcavity. These results suggest a very interesting direction for controlled CND synthesis whereby confinement in nanoscale pores can be used to control the amount of regents and reaction volume size, while the pore morphology (e.g. planar, 3D, linear) can be used to encourage formation of configurations with sp^2 and sp^3 hybridizations and thus to control the structure of the final product. At that, porous $CaCO_3$ as a sacrificial template for CNDs synthesis can be a particularly promising route due to relatively simple precursor uptake and CND extraction.

Methods

Fabrication of $CaCO_3$ microparticles. Uniform, nearly spherical $CaCO_3$ microparticles with narrow size distribution were prepared by colloidal crystallization from supersaturated (relative to $CaCO_3$) solution. The process was initiated by rapid mixing of equal volumes of Na_2CO_3 (Reakhim) *и* $CaCl_2$ ($CaCl_2$:$2H_2O$, Serva) solutions. In a typical experiment, equivalent volumes (0.615 ml) of 1 M Na_2CO_3 and $CaCl_2$ solutions were rapidly poured into the solution of DS (DS, MW 40 kDa, Sigma, concentrations after dilution was 0, 2, 5, and 10 mg/ml) at room temperature. After intense agitation on a magnetic stirrer the precipitate was filtered off, thoroughly washed with bidistilled water and dried in air. The procedure results in highly homogeneous, spherical $CaCO_3$ microparticles with an average diameter ranging from 4 to 6 μm. For hydrothermal treatment $CaCO_3$-DS microparticles obtained in 12 parallel synthesis runs were collected together, dried and placed in a steel autoclave with teflon liner and a heat-resistant glass (Fig. S7). The autoclave was placed in a muffle furnace, heated up to 200 °C at 2.5 °C/min, held for 180 min at this temperature and then cooled. Additional experiments showed that $CaCl_2$ and Na_2CO_3 precipitation leads to DS co-precipitation mainly into $CaCO_3$ microparticles (Table S1). For control

experiments, DS water solutions (4 ml) with concentrations of 2, 5 and 10 mg/ml were hydrothermally treated at the same conditions.

Following the thermal treatment several fractions of carbon material were collected starting from the surface layer towards the centre of $CaCO_3$ microparticles. Surface fraction of CNDs was washed from the $CaCO_3$ microparticles surface with 2 ml of water. CNDs formed inside $CaCO_3$ microparticles pores, were extracted from $CaCO_3$ using HCl solution (0.1 M), which was added step-by-step in fractions of 2 ml. Following each step of NaCl addition, the suspension was shaken, centrifuged (5000 rpm), and the supernatant (fraction) was removed. The process was repeated until the $CaCO_3$ microparticles were completely dissolved. A number of fractions were broadly defined as a surface fraction (fraction 1, obtained from the surface layer), intermediate layer fraction (fraction2, extracted roughly half way towards the particle centre) and the core region (fraction 3, extracted from the core region). All synthesis runs were carried out 3 times and PL was measured. We found that the position of the PL maxima where the same within the experimental error while the intensity variation was no more than 5%.

Experimental Characterization. Measurements of the absorption spectra was carried out using a Shimadzu UV-1800 spectrophotometer (Shimadzu, Japan). PL spectra and excitation-dependent PL were measured using a multifunction fluorimeter Cary Eclipse (Agilent Technologies, Australia).

SEM measurements to characterize the fabricated $CaCO_3$-DS (shape, size, porosity and surface morphology) were performed using MIRA II LMU system (TESCAN, Czech Republic). Ultramicrotome Leica EM UC7 (Leica, Germany) was used to prepare the ultrathin sections of the $CaCO_3$ microparticles to examine their internal structure. For SEM measurements, the water suspension of $CaCO_3$ microparticles was drop-casted onto the silicon wafer and air-dried at room temperature. Prior to the SEM measurements the samples were sputtered with gold. Measurements were performed at operating voltages of 3–30 keV.

Light emission from as-prepared microparticles (before extraction of CNDs) was checked with Leica TCS SP8 X inverted confocal microscope (Leica Microsystems) using Leica 100x/1.44 NA oil N-PLAN objective. The PL was excited by 405 nm laser and the emission λ-scan was recorded from 410 to 750 nm.

Renishaw inVia (Renishaw, UK) Raman confocal microscope equipped with 532 nm and 785 nm lasers was used to acquire the Raman data. Samples were pipetted on gold layer evaporated on Si substrate. The laser beam was focused through a 50x(Leica N PLAN L, NA 0.5) microscope objective and the Raman data were collected in the backscattering mode.

Transmission electron microscopy (TEM) was performed using a JEOL 2010 transmission electron microscope (JEOL, Japan) operated at 200 kV. The system resolution was around 0.2 nm. For the TEM studies, samples in suspension were drop-casted on an ultrathin amorphous carbon film supported on a Cu grid and dried in air.

References

1. Hola, K. *et al*. Carbon dots—Emerging light emitters for bioimaging, cancer therapy and optoelectronics. *Nano Today* **9**, 590–603 (2014).
2. Wang, F., Xie, Z., Zhang, H., Liu, C.-Y. & Zhang, Y.-G. Highly Luminescent Organosilane-Functionalized Carbon Dots. *Adv. Funct. Mater.* **21**, 1027–1031 (2011).
3. Yang, S.-T. *et al*. Carbon Dots as Nontoxic and High-Performance Fluorescence Imaging Agents. *J. Phys. Chem. C* **113**(42), 18110–18114 (2009).
4. Li, H. *et al*. One-step ultrasonic synthesis of water-soluble carbon nanoparticles with excellent photoluminescent properties. *Carbon* **49**(2), 605–609 (2011).
5. Wang, F., Chen, Y.-h, Liu, C.-y & Ma, D.-g. White light-emitting devices based on carbon dots' electroluminescence. *Chem. Commun.* **47**, 3502–3504 (2011).
6. Baker, S. N. & Baker, G. A. Luminescent Carbon Nanodots: Emergent Nanolights. *Angew. Chem. Int. Ed.* **49**, 6726–6744 (2010).
7. Lim, S. Y., Shen, W. & Gao, Z. Carbon quantum dots and their applications. *Chem. Soc. Rev.* **44**, 362–381 (2015).
8. Briscoe, J., Marinovic, A., Sevilla, M., Dunn, S. & Titirici, M. Biomass-Derived Carbon Quantum Dot Sensitizers for Solid-State Nanostructured Solar Cells. *Angew. Chem. Int. Ed.* **54**, 4463–4468 (2015).
9. Zhou, J. *et al*. Facile synthesis of P-doped carbon quantum dots with highly efficient photoluminescence. *RSC Advances* **4**(11), 5465–5468 (2014).
10. Ma, Z., Ming, H., Huang, H., Liu, Y. & Kang, Z. One-step ultrasonic synthesis of fluorescent N-doped carbon dots from glucose and their visible-light sensitive photocatalytic ability. *New J. Chem.* **36**(4), 861–864 (2012).
11. Wei, K., Li, J. J., Ge, Z. S., You, Y. Z. & Xu, H. X. Sonochemical synthesis of highly photoluminescent carbon nanodots. *RSC Advances* **4**(94), 52230–52234 (2014).
12. Yang, P., Zhao, J., Zhang, L., Li, L. & Zhu, Z. Intramolecular hydrogen bonds quench photoluminescence and enhance photocatalytic activity of carbon nanodots. *Chemistry* **21**(23), 8561–8568 (2015).
13. Strauss, V. *et al*. Carbon nanodots: toward a comprehensive understanding of their photoluminescence. *J. Am. Chem. Soc.* **136**(49), 17308–17316 (2014).
14. Wang, X., Qu, K., Xu, B., Ren, J. & Qu, X. Microwave assisted one-step green synthesis of cell-permeable multicolor photoluminescent carbon dots without surface passivation reagents. *J. Mater. Chem.* **21**(8), 2445–2450 (2011).
15. Schwenke, A. M., Hoeppener, S. & Schubert, U. S. Synthesis and modification of carbon nanomaterials utilizing microwave heating. *Adv. Mater.* **27**(28), 4113–4141 (2015).
16. Mitra, S. *et al*. Rapid microwave synthesis of fluorescent hydrophobic carbon dots. *RSC Advances* **2**(32), 12129–12131 (2012).
17. Zhai, X. *et al*. Highly luminescent carbon nanodots by microwave-assisted pyrolysis. *Chem. Commun.* **48**(64), 7955–7957 (2012).
18. Zhu, S. *et al*. Highly photoluminescent carbon dots for multicolor patterning, sensors, and bioimaging. *Angew. Chem. Int. Ed. Engl., V.* **52**(14), 3953–3957 (2013).
19. Barman, M. K., Jana, B., Bhattacharyya, S. & Patra, A. Photophysical properties of doped carbon dots (N, P, and B) and their influence on electron/hole transfer in carbon dots–nickel (II) phthalocyanine conjugates. *J. Phys. Chem. C* **118**(34), 20034–20041 (2014).
20. Guo, Y., Wang, Z., Shao, H. & Jiang, X. Hydrothermal synthesis of highly fluorescent carbon nanoparticles from sodium citrate and their use for the detection of mercury ions. *Carbon* **52**, 583–589 (2013).
21. Song, Y. *et al*. Investigation from chemical structure to photoluminescent mechanism: a type of carbon dots from the pyrolysis of citric acid and an amine. *J. Mater. Chem. C Mater. Opt. Electron. Devices* **3**(23), 5976–5984 (2015).
22. Kim, S. W., Kim, M., Lee, W. Y. & Hyeon, T. Fabrication of hollow palladium spheres and their successful application to the recyclable heterogeneous catalyst for suzuki coupling reactions. *J. Am. Chem. Soc.* **124**, 7642–7643 (2002).

23. Titirici, M. M. & Antonietti, M. Chemistry and materials options of sustainable carbon materials made by hydrothermal carbonization. *Chem. Soc. Rev.* **39**, 103–116 (2010).
24. Goryacheva, I. Y., Sapelkin, A. V. & Sukhorukov, G. B. Carbon nanodots: mechanisms of photoluminescence and principles of application. *Trends in Anal. Chem.* **80**, 27–37 (2017).
25. Tartaj, P., del P Morales, M., Veintemillas-Verdaguer, S., González-Carreño, T. & J Serna, C. The preparation of magnetic nanoparticles for applications in biomedicine. *J. of Phys. D: Applied Phys.* **36**, 182–197 (2003).
26. Yang, Y. H. *et al*. One-step synthesis of amino-functionalized fluorescent carbon nanoparticles by hydrothermal carbonization of chitosan. *Chem. Commun.* **48**, 380–382 (2012).
27. Prasannan, A. & Imae, T. One-Pot Synthesis of Fluorescent Carbon Dots from Orange Waste Peels. *Ind. Eng. Chem. Res.* **52**, 15673–15678 (2013).
28. Wu, Z. L. *et al*. One-pot hydrothermal synthesis of highly luminescent nitrogen-doped amphoteric carbon dots for bioimaging from Bombyx mori silk – natural proteins. *J. Mater. Chem. B.* **1**, 2868–2873 (2013).
29. Yang, Z. C. *et al*. Intrinsically fluorescent carbon dots with tunable emission derived from hydrothermal treatment of glucose in the presence of monopotassium phosphate. *Chem. Commun.* **47**, 11615–11617 (2011).
30. Hu, Y. *et al*. Magnetic Compression of Polyelectrolyte Microcapsules for Controlled Release. *Langmuir* **41**, 11195–11199 (2015).
31. Gouin, S. Microencapsulation: industrial appraisal of existing technologies and trends. *Trends Food Sci. Technol.* **15**, 330–347 (2004).
32. Zhang, L. *et al*. One-Step Microfluidic Fabrication of Polyelectrolyte Microcapsules in Aqueous Conditions for Protein Release. *Angew. Chem.* **128**, 1–6 (2016).
33. Blaiszik, B. J. *et al*. Self-Healing Polymers and Composites. *The Annual Review of Materials Research* **40**, 179–211 (2010).
34. Jing, H. *et al*. Comparison of compounded fragrance and chitosan nanoparticles loaded with fragrance applied in cotton fabrics. *Textile Research J.* **81**, 19 (2011).
35. Zong, J., Zhu, Y., Yang, X., Shen, J. & Li, C. Synthesis of photoluminescent carbogenic dots using mesoporous silica spheres as nanoreactors. *Chem. Comm.* **47**, 764–766 (2011).
36. Sailor, M. J. Fundamentals of Porous Silicon Preparation. *In Porous Silicon in Practice: Preparation, Characterization and Applications* Wiley-VCH Verlag GmbH & Co. KGaA: Weinheim, pp 254 (2012).
37. Chen, Y. Design, Synthesis, Multifunctionalization and Biomedical Applications of Multifunctional Mesoporous Silica-Based Drug Delivery Nanosystems. *Springer Theses*, Springer (2016).
38. Gao, H., Sapelkin, A. V., Titirici, M. M. & Sukhorukov, G. B. *In Situ* Synthesis of Fluorescent Carbon Dots/Polyelectrolyte Nanocomposite Microcapsules with Reduced Permeability and Ultrasound Sensitivity. *ACS Nano* **10**(10), 9608–9615 (2016).
39. Volodkin, D. V., Petrov, A. I., Prevot, M. & Sukhorukov, G. B. Matrix Polyelectrolyte Microcapsules: New System for Macromolecule Encapsulation. *Langmuir* **20**(8), 3398–3406 (2004).
40. Borodina, T. *et al*. Controlled Release of DNA from Self-Degrading Microcapsules. *Macromol. Rapid Commun.* **28**, 1894–1899 (2007).
41. Casanova, H. & Higuita, L. P. Synthesis of calcium carbonate nanoparticles by reactive precipitation using a high pressure jet homogenizer. *Chem Eng. J.* **175**, 569–578 (2011).
42. Biradar, S. *et al*. Calcium carbonate nanoparticles: synthesis, characterization and biocompatibility. *J. Nanosci. Nanotec.h* **11**, 6868–6874 (2011).
43. Hong, K.-S. *et al*. Removal of Heavy Metal Ions by using Calcium Carbonate Extracted from Starfish Treated by Protease and Amylase. *J. of Analytical Science & Technology* **2**(2), 75–82 (2011).
44. Peng, C., Zhao, Q. & Gao, C. Sustained Delivery of Doxorubicin by Porous CaCO3 and Chitosan/Alginate Multilayers-Coated CaCO3 Microparticles. *Colloids and Surfaces A: Physicochemical and Engineering* **353**, 132–139 (2010).
45. De Geest, B. G. *et al*. Degradable Multilayer Films and Hollow Capsules via a 'Click' Strategy. *Macromol. Rapid Commun.* **29**, 1111–1118 (2008).
46. Yoshida, K. *et al*. pH-Dependent Release of Insulin from Layer-by-Layer-Deposited Polyelectrolyte Microcapsules. *Polymers* **7**, 1269–1278 (2015).
47. Sukhorukov, G. *et al*. Porous calcium carbonate microparticles as templates for encapsulation of bioactive compounds. *J. Mater. Chem.* **14**, 2073–2081 (2004).
48. Deng, J., Lu, Q., Li, H., Zhang, Y. & Yao, S. Large scale preparation of graphene quantum dots from graphite oxide in pure water via one-step electrochemical tailoring. *RSC Adv.* **5**, 29704 (2015).
49. Hernandez, Y. *et al*. High-yield production of graphene by liquid-phase exfoliation of graphite. *Nature nanotechnology* **3**, 563–568 (2008).
50. Casiraghi, C., Ferrari, A. C. & Robertson, J. Raman spectroscopy of hydrogenated amorphous carbons. *Phys. Rev. B.* **61**, 14095 (2000).
51. Ghandour, A. J. *et al*. Pressure coefficients of Raman modes of carbon nanotubes resolved by chirality: Environmental effect on graphene sheet. *Phys. Rev. B.* **87**, 085416 (2013).
52. Zhan, D. *et al*. Electronic structure of graphite oxide and thermally reduced graphite oxide. *Carbon* **49**, 1362–1366 (2011).
53. Yuan, R., Yuan, J., Wu, Y., Chen, L. & Zhou, H. Chen, Efficient synthesis of graphene oxide, and the mechanisms of oxidation and exfoliation. *J. App. Surf. Sci.* **416**, 868–877 (2017).
54. May, P. W., Mankelevich Y. A. Experiment and modeling of the deposition of ultrananocrystalline diamond films using hot filament chemical vapor deposition and Ar/CH4/H2 gas mixtures: A generalized mechanism for ultrananocrystalline diamond growth. *J. Appl. Phys.* **100**, 024301-024301-9 (2006).
55. May, P. W., Smith, J. A. & Mankelevich, Yu Deposition of NCD films using hot filament CVD and Ar/CH4/H2 gas mixture. *Diamond and Related Materials.* **15**(2), 345–352 (2006).
56. Marshall, C. P. & Marshall, A. O. Trans Phil. The potential of Raman spectroscopy for the analysis of diagenetically transformed carotenoids. *R. Soc.* **368**, 3137–3144 (2010).
57. Vinh, L. D., Abenoza, M. & Rault, J. Etude des modes Raman de déformation angulaire des CH2 dans le polyethylene. *J. Phys. France* **40**, 597–605 (1979).

Acknowledgements

This work has been supported by the Russian Science Foundation grant number 16-13-10195. TEM work has been supported by the Biological Sciences Research Council grant BB/J001473/1.

Author Contributions

A.V.V. carried out synthesis, absorption and PL spectra, prepared supporting information and Figure 1; E.S.P. carried out Raman measurements, O.A.M. carried out synthesis; I.Y.G. contributed to discussions and text preparation; N.V.T. carried out TEM measurements, analysis and prepared TEM images; G.B.S. contributed to discussions and text preparation; A.V.S. contributed to discussions, text preparation, contributed to preparation of Figure 2 and Figure 3. The manuscript was written through contributions of all authors.

Additional Information

Supplementary information accompanies this paper at https://doi.org/10.1038/s41598-018-27488-w.

Competing Interests: The authors declare no competing interests.

Publisher's note: Springer Nature remains neutral with regard to jurisdictional claims in published maps and institutional affiliations.